Table 1. $\sin^2(\alpha/2)$ *values for two types of DC's for various reflections*

h	k	l	$\alpha_1(°)$	$\alpha_2(°)$	$\sin^2(\alpha_1/2)$	$\sin^2(\alpha_2/2)$
2	0	$-\frac{2}{3}$	312·7	72·5	0·161	0·350
2	0	$-\frac{4}{3}$	−96·5	23·4	0·556	0·411
2	0	$\frac{2}{3}$	72·5	312·7	0·350	0·161
−2	0	$\frac{2}{3}$	312·7	72·5	0·161	0·350
−2	0	$-\frac{2}{3}$	72·5	312·7	0·350	0·161

from Table 1, in agreement with the observations. Fig. 7 is the case between the $\bar{2}0\frac{2}{3}$ and $20\frac{2}{3}$, and contrast reversal is not expected, again in agreement with the observations.

From the discussion here it can be said that if the direction of P_s in one domain, say domain 1 in Fig. 3 or 8, is determined by the method mentioned in § 4.2 it will be possible to differentiate a configuration of domains in the order shown in Fig. 8 from that in the reverse order by the contrast analysis of the DC's.

4.4. *Electron diffraction in the IC phase*

From the structural relations between the lattices of the successive domains diffraction spot distributions in the IC phase can be calculated. It was found that asymmetric splitting of the superlattice reflections and their relative intensities were well reproduced.

The authors thank Professor K. Hamano of the Tokyo Institute of Technology for his kind supply of the sample crystals.

References

AMELINCKX, S. (1970). *Modern Diffraction and Imaging Techniques in Material Science*, edited by S. AMELINCKX, R. GEVERS, G. REMAUT & J. VAN LANDUYT, pp. 257-294. Amsterdam: North Holland.

BESTGEN, H. (1986). *Solid State Commun.* **58**, 197-201.

CHEN, C. H., GIBSON, G. M. & FLEMING, R. M. (1982). *Phys. Rev. B*, **26**, 184-205.

DOLINO, G., BACHHEIMER, J. P., BERGE, B., ZEYENK, C. M. E., VAN TENDELOO, G., VAN LANDUYT, J. & AMELINCKX, S. (1984). *J. Phys. (Paris)*, **45**, 901-912.

FUJINO, Y., SATO, H., HIRABAYASHI, M., AOYAGI, E. & KOYAMA, Y. (1987). *Phys. Rev. Lett.* **58**, 1012-1015.

FUNG, K. K., MCKERNAN, S., STEEDS, J. W. & WILSON, J. A. (1981). *J. Phys. C*, **14**, 5417-5432.

ISHIBASHI, Y. (1986). *Incommensurate Phases in Dielectric Materials*, edited by R. BLINC & A. P. LEVANYUK, pp. 49-69. Amsterdam: North Holland.

ITOH, K. *et al.* (1986). Private communication.

MCMILLAN, W. L. (1975). *Phys. Rev. B*, **12**, 1187-1199.

MAHY, J., VAN LANDUYT, J., AMELINCKX, S., UCHIDA, Y., BRONSEMA, K. D. & VAN SMAALEN, S. (1985). *Phys. Rev. Lett.* **55**, 1188-1191.

TANAKA, M. & HONJO, G. (1964). *J. Phys. Soc. Jpn*, **19**, 954-970.

TSUDA, K., YAMAMOTO, N. & YAGI, K. (1988). *J. Phys. Soc. Jpn*, **57**. In the press.

TSUDA, K., YAMAMOTO, N., YAGI, K. & HAMANO, K. (1986). Proc. 11th Int. Congr. Electron Microscopy (Kyoto), Vol. 2, pp. 1233-1234.

VAN TENDELOO, G. & AMELINCKX, S. (1974). *Acta Cryst.* A**30**, 431-440.

YAMAMOTO, N., TSUDA, K. & YAGI, K. (1985). *Jpn. J. Appl. Phys.* **24**, Suppl. 2, 811-813.

YAMAMOTO, N., TSUDA, K. & YAGI, K. (1988). *J. Phys. Soc. Jpn*, **57**, 1352-1364.

YAMAMOTO, N., YAGI, K. & HONJO, G. (1977). *Phys. Status Solidi A*, **44**, 147-160.

Acta Cryst. (1988). A**44**, 870-878

Electron Diffraction Analysis of Polycrystalline and Amorphous Thin Films

BY D. J. H. COCKAYNE

Electron Microscope Unit, University of Sydney, NSW 2006, *Australia*

AND D. R. MCKENZIE

School of Physics, University of Sydney, NSW 2006, *Australia*

(*Received* 12 *January* 1988; *accepted* 25 *April* 1988)

Abstract

A rapid analytical technique has been developed for obtaining the reduced density function, $G(r)$, from polycrystalline and amorphous thin films, using post-specimen scanning and an energy loss spectrometer on a transmission electron microscope. The technique gives on-line analysis of nearest-neighbour distances to an accuracy of 0·02 Å, together with coordination numbers. It has the advantage over X-ray and neutron techniques that the information can be obtained from small (≤ 1 μm diameter) chosen regions of the specimen. Results from neighbouring selected regions can be compared.

1. Introduction

If one were to look for a common thread in the work, so far, of J. M. Cowley and of A. F. Moodie, whether severally or in tandem, it would be found in the

0108-7673/88/060870-09$03.00

application of mathematical techniques combined with electron optical innovations to the elucidation of structure. It is this combination of theory and experiment which has excited the physicist, and the results of which have enthused the materials scientist. In this spirit of combining mathematics with developments in electron optics, this paper is dedicated to Cowley and Moodie for the enthusiasm and excitement that they have brought to the field.

Thin films deposited by physical and chemical vapour deposition techniques often show an amorphous or polycrystalline structure of small grain size, so that the selected area diffraction pattern from regions of 10 μm or larger is a series of concentric rings. In this work we shall further restrict our attention to specimens which show no preferred orientation effects, and which therefore give a circularly symmetric diffraction pattern.

Electron diffraction has a number of advantages over other forms of radiation for the structural investigation of thin films. The most important of these is the large scattering cross section which, combined with the availability of intense beams, permits rapid data collection with good statistics. Additionally the small wavelength compared with X-rays and neutrons allows collection of data to large values of $s = 2(\sin\theta)/\lambda$, and hence good resolution in real space. Against this, electron diffraction cameras, and electron microscopes operated in the diffraction mode in particular, must generally be calibrated against a crystalline standard - a process which is not necessary for X-rays and neutrons.

A great deal of work has been reported using photographic recording of electron diffraction patterns. This allows parallel recording of intensity, that is, the recording of intensities at all scattering angles simultaneously, but it introduces the difficulty of recording intensities which have a large dynamic range using a medium which has a non-linear response. In addition to this problem, many methods of analysing the data assume that the diffraction pattern contains only elastically scattered electrons. In general this is an unreasonable assumption for all but the thinnest films.

There have been a number of previous attempts to overcome these difficulties by collecting energy-filtered electron diffraction patterns sequentially. Grigson (1962) described a system in which the diffraction pattern formed by an electron microscope is energy filtered by a retarding potential near the plane of the viewing screen. A similar system using electrostatic filtering has been described by Graczyk & Moss (1969), who applied their instrument to studies of amorphous silicon (Moss & Graczyk, 1969). However, in general, the difficulties mentioned above have meant that the full potential of electron diffraction for the investigation of amorphous and polycrystalline thin films has not been realized.

This paper describes a complete experimental and analytical system which overcomes these problems, and which can produce rapid on-line determinations of the reduced density function $G(r)$, which displays nearest-neighbour distances and gives coordination numbers. The system makes use of commercially available electron energy loss spectrometers attached to an electron microscope, and this provides an ideal means of obtaining the energy-filtered electron diffraction patterns. It is our belief that the ability to obtain rapid (2 to 4 min) on-line nearest-neighbour data will make electron diffraction analysis of thin amorphous and polycrystalline films a widely used analytical technique.

2. Theory

2.1. *Reduced density function*

Following Warren (1969), the scattered intensity for the scattering vector **s**, with modulus $s = 2(\sin\theta)/\lambda$, for a sample with atoms at positions $\mathbf{r}_i$, is

$$I(s) = \sum_m f_m^2 + \sum_m f_m \sum_{n \neq m} f_n \exp(2\pi i \mathbf{s}.\mathbf{r}_{nm})$$

where $\mathbf{r}_{nm} = \mathbf{r}_n - \mathbf{r}_m$. Let $\rho_{mj}(\mathbf{r}_{nm})\,\mathrm{d}V_n$ be the density of atoms of type j in the volume element $\mathrm{d}V_n$ at position $\mathbf{r}_{nm}$ around atom m. Then

$$I(s) = \sum_m f_m^2 + \sum_j \sum_{m \neq n} f_m \int_S f_n \rho_{mj}(\mathbf{r}_{nm}) \times \exp[2\pi i(\mathbf{s}.\mathbf{r}_{nm})]\,\mathrm{d}V_n$$

where the integral is evaluated over the entire sample. Let the average density of type j atoms be ρ_j and let there be N_j atoms of type j with scattering factor f_j in the sample. Then

$$I(s) = \sum_j N_j f_j^2 + \sum_j \sum_{m \neq n} f_m \times \int_S f_j[\rho_{mj}(\mathbf{r}_{nm}) - \rho_j] \exp[2\pi i(\mathbf{s}.\mathbf{r}_{nm})]\,\mathrm{d}V_n + \sum_j \sum_{m \neq n} f_m f_j \rho_j \int_S \exp[2\pi i(\mathbf{s}.\mathbf{r}_{nm})]\,\mathrm{d}V_n.$$

The integral of the third term depends upon the shape of the specimen, and gives rise to small-angle scattering which will be discussed in § 4.2. Taking $I'(s)$ to be $I(s)$ with the small-angle scattering neglected, we have

$$I'(s) = \sum_j N_j f_j^2 + \sum_j \sum_{m \neq n} f_m \times \int_S f_j[\rho_{mj}(\mathbf{r}_{nm}) - \rho_j] \exp[2\pi i(\mathbf{s}.\mathbf{r}_{nm})]\,\mathrm{d}V_n.$$

Considering a particular $\mathbf{r}_{nm} = \mathbf{r}$, we let $\rho_{ij}(\mathbf{r})$ be the average value of $\rho_{mj}(\mathbf{r}_{nm})$ averaged over all atoms m of type i. Further, for an amorphous sample, $\rho_{ij}(\mathbf{r}) - \rho_j$ approaches zero for $|\mathbf{r}|$ greater than a few atomic distances. Hence, assuming no preferred orientation,

we obtain

$$I'(s)=\sum_j N_j f_j^2+\sum_j\sum_i N_i f_i \times\int_0^\infty f_j[\rho_{ij}(r)-\rho_j]2r\sin(2\pi sr)/s\,dr$$

where $r=|\mathbf{r}|$.

We introduce the quantities

$$\langle f\rangle^2=\left(\sum_i N_i f_i\right)^2\Big/N^2 \quad\text{and}\quad \langle f^2\rangle=\sum_i N_i f_i^2\Big/N$$

where

$$N=\sum_i N_i.$$

Then

$$I'(s)=N\langle f^2\rangle+\int_0^\infty\sum_j\sum_i N_i f_i f_j \times[\rho_{ij}(r)-\rho_j]2r\,[\sin(2\pi sr)/s]\,dr.$$

Let

$$\rho^R(r,s)\equiv\left[\sum_j\sum_i N_i f_i f_j\rho_{ij}(r)\right]\Big/N\langle f\rangle^2. \qquad (1)$$

Then

$$I'(s)=N\langle f^2\rangle+\int_0^\infty\left[N\langle f\rangle^2\rho^R(r,s)-\sum_j\sum_i N_i f_i f_j\rho_j\right]\times 2r\,[\sin(2\pi sr)/s]\,dr.$$

But $N_i/N=\rho_i/\rho_0$ where $\rho_0=\sum_i\rho_i$. Then

$$\sum_j\sum_i N_i f_i f_j\rho_j=\left(\sum_i N_i f_i\right)\left(\sum_j f_j\rho_j\right)=N\rho_0\langle f\rangle^2.$$

So

$$I'(s)=N\langle f^2\rangle+N\langle f\rangle^2\int_0^\infty[\rho^R(r,s)-\rho_0]\times 2r\,[\sin(2\pi sr)/s]\,dr.$$

A reduced intensity function is defined by

$$\varphi(s)=[I'(s)-N\langle f^2\rangle]s/N\langle f\rangle^2=\int_0^\infty 2r[\rho^R(r,s)-\rho_0]\sin(2\pi sr)\,dr. \qquad (2)$$

This is Fourier invertible if

$$f_i=K_i f \qquad (3)$$

where $f=f(s)$, and K_i is a constant independent of s, since then $\rho^R(r,s)\equiv\rho^R(r)$. This assumption is discussed in § 5.2.

Then Fourier inversion yields the reduced density function (RDF)

$$G(r)=4\pi r[\rho^R(r)-\rho_0]=8\pi\int_0^\infty\varphi(s)\sin(2\pi sr)\,ds. \qquad (4)$$

The function $G(r)$ describes the deviation of $\rho^R(r)$ from ρ_0, the total atom density in the sample. From (1), a maximum in $\rho^R(r)$ [and hence in $G(r)$] will correspond to a maximum in an individual $\rho_{ij}(r)$, say $\rho_{kl}(r)$, if the $\rho_{ij}(r)$ do not overlap. Under these conditions, maxima in $G(r)$ give the most probable distances between atoms of types k and l. The identification of these distances with particular types of atom can often be inferred from a knowledge of relevant crystalline structures.

In practice, this procedure for determining most probable distances and atom types can be used even when there is a small degree of overlap, and, if necessary, deconvolution can be employed. In the case of severe overlap resulting in ambiguity in the interpretation of the maxima in $G(r)$, it is necessary to use more than one kind of radiation (*e.g.* X-rays and neutrons) in order to evaluate the ρ_{ij} independently of each other (*e.g.* Keating, 1963).

2.2. *Coordination numbers*

If it is possible to ascribe a given maximum in $G(r)$ to the interatomic distance r between two types of atom i and j, as discussed above, then we can calculate the average coordination number C_{ii} of type i atoms about a type i atom, by evaluating the integral

$$C_{ii}(r_1,r_2)=\int_{r_1}^{r_2}4\pi r^2\rho_{ii}(r)\,dr$$

where r_1 and r_2 are the distance limits which are to be associated with the specified interatomic distance. From (1) and (3)

$$C_{ii}(r_1,r_2)=\int_{r_1}^{r_2}\frac{4\pi r^2N\langle f\rangle^2}{N_iK_i^2f^2}\rho^R(r)\,dr=\frac{N\langle f\rangle^2}{N_iK_i^2f^2}\int_{r_1}^{r_2}4\pi r^2\rho^R(r)\,dr=\frac{N\langle f\rangle^2}{N_iK_i^2f^2}\left[\int_{r_1}^{r_2}rG(r)\,dr+\tfrac{4}{3}\pi\rho_0(r_2^3-r_1^3)\right].$$

For the case of $i\neq j$, we define an 'average mutual coordination coefficient' C_{ij} where

$$C_{ij}(r_1,r_2)=\int_{r_1}^{r_2}\frac{4\pi r^2}{(N_i+N_j)}[N_j\rho_{ij}(r)+N_i\rho_{ji}(r)]\,dr=\frac{N\langle f\rangle^2}{(N_i+N_j)K_iK_jf^2}\left[\int_{r_1}^{r_2}rG(r)\,dr+\tfrac{4}{3}\pi\rho_0(r_2^3-r_1^3)\right]. \qquad (5)$$

2.3. *Multiple scattering*

The derivations of expressions for $G(r)$ and coordination numbers in the previous sections assume single electron scattering. Whether this is a reasonable

assumption in a particular experiment depends upon the specimen thickness, D, and the elastic mean free path Λ. If $S(s)$ is the single scattering distribution, then

$$I(s) = [\delta(s) + (D/\Lambda)S(s) + (1/2!)(D/\Lambda)^2 S(s) * S(s) + \ldots] \exp(-D/\Lambda) \quad (6)$$

where the nth-order convolution refers to nth-order scattering (Egerton, 1986).

It is seen that the important parameter is D/Λ, and that the accuracy of the single-scattering assumption depends upon its magnitude and the form of $S(s)$. Λ is a function of the material and the incident electron energy and increases with increasing energy and decreasing ρ_0 and z, where z is the atomic number. The effects of multiple scattering can be minimized either by choosing parameters of D and electron energy such that multiple scattering is negligible, or by deconvolution techniques [see for example Fourier log deconvolution in Egerton (1986)].

The effect of multiple scattering upon the diffraction patterns of the kind discussed here is to transfer intensity from small to large values of s, and can be recognized by $N\langle f^2\rangle$ being significantly larger than $I(s)$ for small s when fitted at large s by using N as a variable parameter. By performing the analysis on both $I(s)$ and $S(s)$ of (6), Anstis, Liu & Lake (1988) have demonstrated that, for a typical polycrystalline Pt specimen, multiple scattering has only an insignificant effect upon positions of peaks of $G(r)$ for $D/\Lambda \leqslant 5$, but a significant effect for the determination of coordination numbers.

In the experiments reported here, multiple-scattering effects have been minimized by the use of a high electron accelerating voltage (300 kV) and thin specimens. The advantages of higher voltage are evident from the values Λ (100 kV)/Λ (300 kV) = 0·4, 0·5 and 0·6 for C, Ge and Pt respectively (Reimer, 1984).

3. Instrumentation

The system described here was developed for the convenient and rapid on-line collection and processing of diffraction data from selected regions of an amorphous or polycrystalline specimen, to obtain the real-space distances present in the specimen. A conventional transmission electron microscope (Philips EM430) is used to project a selected area diffraction pattern onto the entrance plane of an energy-selecting spectrometer (Gatan EELS 607) collecting in a serial mode. The diffraction pattern is scanned stepwise across the entrance aperture of the spectrometer, with the spectrometer set to receive electrons of a chosen energy range. The diffraction pattern is then displayed and stored as the sequential output of the spectrometer.

Scanning of the diffraction pattern can be done by deflection coils positioned at any convenient point in the electron microscope column. Earlier work (*e.g.* Grigson, 1962) used deflection plates placed in the region of the entrance aperture. In the work reported here, post-specimen scan coils positioned close to the back focal plane of the objective lens are used. In using this method, it is important to ensure that the energy selected by the spectrometer remains steady as the diffraction pattern is translated. This can place severe electron-optical requirements on the optics of the system. An alternative method is to vary the incident-beam direction by using beam-tilting coils above the specimen. A difficulty with this method is to obtain a sufficiently large beam tilt without a change in the area of the specimen illuminated. We have used the first of these methods on a Philips EM430 transmission microscope, and the second on a JEOL 100C. The post-specimen scanning, which is available on most modern microscopes, gives more reliable data, and is more convenient.

The scanning and data collection are accomplished under computer control. The computer provides a ramp output which is directed to the scan coils through an appropriate interface. (In the case of the Philips EM430, the 'hybrid diffraction unit' provides a convenient means for doing this.) A convenient ramp control is that provided by the operating system for ramping the magnet on a serial energy loss spectrometer. If this is used, then the output from the spectrometer can be manipulated using the operating-system software.

In our system, the diffraction pattern is centred on the spectrometer entrance aperture, and scanned from large to small s to avoid saturating the detector. The centre of the diffraction pattern is found by including in the scan a major feature appearing symmetrically on each side of $s = 0$. Inaccuracy in determining the centre results in an error in determining s_{max} which in turn results in a scaling error of r in $G(r)$. Resolution in s space depends upon the step size in s, the size of the diffraction pattern and the diameter of the spectrometer entrance aperture. It depends also upon the convergence angle of the incident electron beam, as determined by the settings of the condenser lenses.

Equation (4) is derived for elastic scattering, but in practice a range of energies must be collected. Of necessity, thermal diffuse scattering is always included with the system described here, and in practice an energy window of 3 to 6 eV is chosen. The main experimental limitation in choosing smaller widths of the window is the drift of the energy loss spectrum during the collection time. It is clearly important the energy window should not include any plasmon scattering.

With this system, a typical collection time for the diffraction pattern shown in Fig. 1 is 2 min for 1024 data points.

4. Numerical procedures

A number of numerical procedures are involved in collecting the data to produce $\varphi(s)$ [(2)], and in reducing and transforming it to derive $G(r)$ [(4)]. These procedures, and their associated approximations and errors, are discussed in turn.

4.1. *Calibration*

The intensity $I(s)$ is collected into a multi-channel analyser by scanning the diffraction pattern across the entrance aperture of an energy selecting spectrometer. Linearity in s requires that the scanned increments are equally spaced in s, or if not, then that they are calibrated. To check the linearity, maxima in the diffraction pattern of polycrystalline Pt were identified to $s = 2{\cdot}32$ Å^{-1} (corresponding to the 753 reflection) from its face-centred cubic structure. By collecting a number of patterns with different incident-beam directions, the linearity of the scan over the full range to $s = 5{\cdot}0$ Å^{-1} was found to be better than 0·5%.

The linearity of the measured intensity $I(s)$ with count rate was tested by collecting identical Pt diffraction patterns for a range of incident beam intensities. For a peak with a count rate of 10^6 counts s^{-1}, the reduction in counts was found to be 19%, reducing to 5% for a count rate of 2×10^5 counts s^{-1}. This error, which is due to the dead time of the detector, can be reduced to any desired value by multiple scans at a sufficiently low count rate, or, if necessary, can be compensated for.

4.2. *Small-angle scattering*

There are two contributions to $I(s)$ for $s \leqslant 0{\cdot}1$ Å^{-1} which have been ignored in the derivation of $G(r)$. These are the small-angle scattering due to the finite size of the scattering volume, and the unscattered beam which extends to non-zero s because of the optics of the system. In the system described in this paper, these two contributions result in a narrow peak in $\varphi(s)$ near $s \simeq 0{\cdot}03$ Å^{-1}. Fourier transformation of this peak to obtain $G(r)$ results in an oscillation of period $\simeq 33$ Å. This slow variation in $G(r)$ can be recognized easily, and can be removed by eliminating the feature from $\varphi(s)$ before transformation.

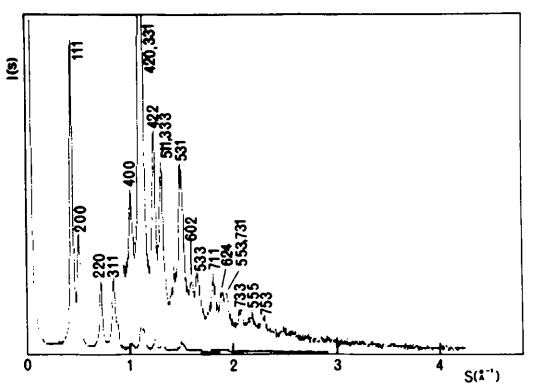

Fig. 1. A polycrystalline Pt diffraction pattern (with scale change) collected with 300 kV electrons.

4.3. *Formation of $\varphi(s)$ and $G(r)$*

The terms $\langle f \rangle^2$ and $\langle f^2 \rangle$ in (2) are evaluated using the tabulated electron scattering factors given by Doyle & Turner (1968), with the composition of the specimen being obtained from electron energy loss or X-ray energy dispersive analysis, or from prior knowledge. Values of f intermediate to those tabulated by Doyle & Turner (1968) are determined by fitting a spline function. The value of N in (2) is usually chosen to minimize the oscillations in $G(r)$ at small r (typically $r < 1{\cdot}5$ Å). Kaplow, Strong & Averbach (1965) have discussed the justification for this procedure. The success of the minimization seems to be element dependent. However, it should be pointed out that a less than optimum value of N results in an oscillatory form of $G(r)$ at small r, as described above (and see Fig. 6), and this is not important in determining the positions of peaks in $G(r)$ for $r > 1{\cdot}5$ Å. However, the choice of N is important if coordination numbers are to be extracted from the data (see § 5.1) since the magnitude of $G(r)$ is scaled by the parameter N.

Once we have determined the parameters for (2), $\varphi(s)$ is formed. The integral of (4) is carried out using a fast Fourier transform (FFT) routine, but must be terminated at $s = s_{max}$, where s_{max} is the limit of the data collected. This is determined by the collection geometry and in our case is $\simeq 5$ Å^{-1}. This termination results in a loss of resolution in $G(r)$, since $G(r)$ obtained for infinite s is convoluted with an Airy function of full width $1/s_{max}$. For example, a function $G(r) = \delta(r - r_0)$ would become a peak of full width $1/s_{max}$ at $r = r_0$. In our case, this width is $\sim 0{\cdot}2$ Å. The position of this peak is not altered by the termination at s_{max}, and can be determined by suitable peak fitting. In addition to loss of resolution, terminating the data at s_{max} results in additional oscillations in $G(r)$ at small r.

The usefulness of the data to $s = s_{max}$ depends upon the specimen and the collection conditions. The statistical significance of data for large s can be improved by using longer counting times or repeated scans. This has not been done for the example of Fig. 1.

The Fourier sine transform of (4) is carried out as a discrete transform using the routine FFT given by Brigham (1974). The routine has been adapted to give a $2N$-point Fourier sine transform by carrying out an N-point complex transform. If the 1024 points of data at equally spaced values of s to s_{max} are used as input, the transform is available only at values of r

spaced at increments of $1/s_{max}$. A convenient interpolation is obtained by extending the data with zeroes to values beyond s_{max}. We have found an extension to $4s_{max}$, or 4096 data points, gives a convenient sampling of the transform enabling the positions of peaks to be obtained with improved accuracy.

Before we carry out the Fourier sine transform, a damping factor $\exp(-Bs^2)$ is applied to $\varphi(s)$. This is necessary to reduce the effects of noise in $I(s)$, which are accentuated in $\varphi(s)$ at large s because of the multiplying factor s and because of the dividing factor $N\langle f\rangle^2$ [(2)]. This procedure, which is routine in reduced density function (RDF) analysis, is discussed in detail by Warren (1969). A typical value of B is 0·2 Å^2, but the choice depends upon the statistics in a given experiment.

A number of systematic studies have been made of the sources of error in RDF analysis, and techniques for minimizing their effect have been described. Konnert & Karle (1973), Grigorovici (1973) and Kaplow, Strong & Averbach (1965) have described iterative procedures which produce a RDF essentially free from termination and background errors. These procedures rely upon methods for choosing representations of the terms $N\langle f\rangle^2$ and $N\langle f^2\rangle$ and upon using *a priori* knowledge that $G(r) = -4\pi\rho_0 r$ for small r. These iterative techniques are yet to be applied using our system, but are likely to improve further the result for $G(r)$ by eliminating small spurious oscillations which are evident for $r <$ 1·5 Å in some of the $G(r)$ presented in this paper.

5. Experimental applications

5.1. *Polycrystalline* Pt

To test the accuracy of the experimental and numerical system described here, a study has been made of thin polycrystalline Pt films prepared by vacuum evaporation onto a KCl substrate, for which the structure is known. The film was floated onto the surface of distilled water, and collected onto a 400 mesh copper electron microscope specimen grid. Fig. 1 shows $I(s)$ collected to $s \simeq 4{\cdot}8$ Å^{-1}, with the peaks in $I(s)$ identified. (It is worth noting that, although the calibration of s is carried out for each data set, in the system described here the range of the collection over s has been found to be invariant to one data channel in 1024.) An approximate value of N was obtained by matching Nf^2 to $I(s)$ at large s, with N as a variable parameter. $\varphi(s)$ was then formed, and $G(r)$ obtained using a damping factor $B =$ 0·25 Å^2. The procedure was repeated for slightly different values of N, and an optimum value of N chosen as being the value of N which minimized oscillations in $G(r)$ for small r (see § 4.3).

$\varphi(s)$ and $G(r)$ for this value of N (=205 in arbitrary units) are shown in Fig. 2, together with $G(r)$ for N close to the optimum value. The oscillations close to $r = 0$ used to optimize N are apparent.

Table 1. *The experimentally measured nearest-neighbour positions in* Pt *compared with theoretical values*

Peak number	Measured r (Å)	Theoretical r (Å)
1	2·79	2·77
2	3·94	3·92
3	4·82	4·81
4	5·56	5·55
5	6·24	6·20
6	6·81	6·80
7	7·37	7·34

Table 1 shows peak positions in $G(r)$ compared with theoretical values of nearest neighbours determined from the f.c.c. structure of Pt with $a = 3{\cdot}914$ Å. It is seen that the experimentally determined values are accurate to 0·7%. The slope of $G(r)$ at $r = 0$ is $-4\pi\rho_0 r$ [(4)], and from this the data in Fig. 2 give $\rho_0 = 0{\cdot}05$ (1) atoms Å^{-3}, which is close to the crystalline density of 0·067 atoms Å^{-3}.

Coordination numbers were calculated from (5), which reduces to

$$C_{11}(r_1, r_2) = \int_{r_1}^{r_2} rG(r)\,dr + 4\pi\rho_0(r_2^3 - r_1^3).$$

There is some latitude in choosing r_1 and r_2. Choosing the values where $G(r)$ intercepts the line $-4\pi\rho_0 r$ includes the range where $\rho(r) > 0$, but such a choice is not always possible, especially for higher values of r or for regions of peak overlap.

For the first peak in Fig. 2, such a choice of r_1 and r_2 is possible and gives $C_{11} = 12{\cdot}10$, which is reasonably close to the 12 first-nearest neighbours.

As explained in § 4.3, and in detail by Kaplow, Strong & Averbach (1965), the scale of $G(r)$ (and

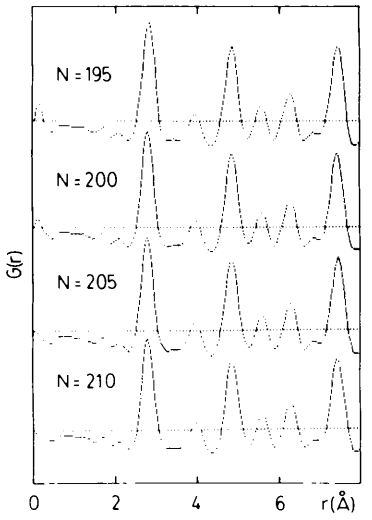

Fig. 2. $G(r)$ obtained for different values of the scaling parameter N for a Pt specimen.

hence the calculated coordination number) is sensitive to the choice of N. Fig. 3 shows this dependence, and it is seen that the theoretical value for C_{11} of 12 is obtained for a value of N (=207·5) very close to that chosen by optimizing for minimum oscillations in $G(r)$ at small r ($N = 205$). This result demonstrates the suitability of using this technique for choosing N.

5.2. *Binary alloy of* Si *and* F

In this section the techniques for extracting coordination data for a binary alloy are illustrated, with reference to a model system of Si and F, as studied by Lake (1988). A model system is used, rather than experimental data, so that the coordination number obtained from a generated $I(s)$, using the numerical analysis, can be compared with the known coordination number of the model. In this way, the usefulness of the approximation that the two scattering factors are related by a constant of proportionality can be studied. The model system consists of crystallites of cubic SiC in which C is replaced by F. The Debye formula was used to calculate $I(s)$ from the assumed structure, using the scattering factors of Doyle & Turner (1968) and a crystallite size of 64 atoms.

The analysis of § 2 was followed, where f is the scattering factor of silicon, $N_i = N_j = N/2$, $K_1 = 1$, and K_2 is to be determined. The analysis of § 2 assumes that the scattering factors of silicon and fluorine differ throughout the range of s only by a constant scale factor K_2. However, this is an approximation and so an optimum value of K_2 has to be found.

The values of C_{12} for the first three nearest neighbours, determined from (5) and the simulated $I(s)$, are 2·71, 8·04 and 8·00. The theoretical values for C_{12} for the model structure are obtained by replacing each F by Si, and repeating the above analysis with $K_2 = 1$. This gives coordination numbers of 2·89, 7·96 and 7·71. These values are less than the infinite crystal values (*e.g.* 4 for the first-nearest neighbour) because of the finite site of the crystallites in the assumed model structure. The choice of $K_2 = 0{\cdot}63$ was made to give the best fit for the first three nearest neighbours, and it is seen (Fig. 4) that this optimum value matches the two scattering factors at large s ($s \geq 2\ \text{Å}^{-1}$). The discrepancies between the two sets of values reflect the consequences of assuming that the scattering factors are proportional. It is apparent from (5) that C_{12} is proportional to $1/K_2$, and consequently the effect of choosing different values of K_2 is clear. Nevertheless analyses show that choosing K_2 in the way proposed here is preferable to choosing K_2 to match the scattering factors at $s = 0$ (Graczyk, 1979). If this latter choice is made, a value of $K_2 = 0{\cdot}31$ is obtained, resulting in an error of 30% in C_{12} for the first-nearest neighbour.

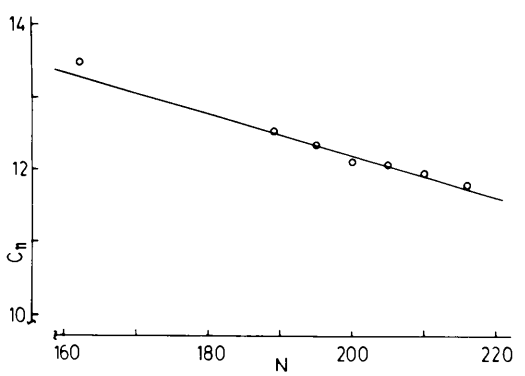

Fig. 3. C_{11} obtained for polycrystalline Pt using N [equation (2)] as a variable parameter. The f.c.c. value is $C_{11} = 12$.

5.3. *Differentiating between alternative structures*

As examples of the use of $G(r)$ to deduce structural information which is not readily apparent from the diffraction pattern itself, results of studies using $G(r)$ to differentiate between a small number of possible alternative structures are discussed.

Thin specimens of glassy carbon, a-Ge and a-Si:H were prepared, the first from resin pyrolysis (Jenkins & Kawamura, 1976), the second by vacuum evaporation and the third by glow discharge in silane. The short-range order in a-Ge and a-Si:H follows the diamond structure. The $G(r)$ determined for these two materials are shown in Figs. 5(*a*) and (*b*). The short-range order for the glassy carbon produces the $G(r)$ shown in Fig. 5(*c*). This material has a local order based on graphite layers. Measurement of the peak positions can be used to give structural parameters, but qualitatively the $G(r)$ for these two structures differ clearly in the small shoulder on the high-r side of the second peak and in the doubling of the third peak, for the graphite-based structure compared with the diamond-based structure. These features can be correlated with the nearest-neighbour distances in the two structures, and can be used as a fingerprint to decide which of the two structures applies for a specimen of unknown structure.

As examples, Fig. 5(*d*) shows $G(r)$ obtained from a BN specimen prepared by ion-beam synthesis

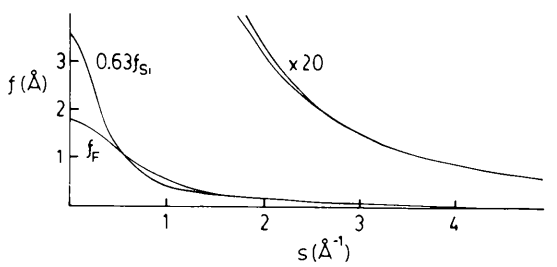

Fig. 4. Scattering factors f for silicon and for fluorine (scaled), showing the scaling of fluorine which gives the best values for the first three coordination numbers for test data (see text).

Table 2. *Peak widths and widths/bond length, determined from $G(r)$ for the materials shown*

Material	First peak width (half-height) Å	Deconvoluted width of second peak (Å)	Second-nearest neighbour bond length (Å)	Width/bond length
a-Ge	0·29	0·52	4·00	0·13
a-Ge:H	0·27	0·52	4·00	0·13
a-Si:H	0·30	0·49	3·90	0·12
a-C	0·32	0·28	2·54	0·11
a-SiC	0·40	0·42	3·10	0·13
Pt	0·30	—	—	—

E.s.d.'s: bond length ±0·02 Å; second peak width ±0·02 Å; width/bond length ±0·006.

(Sainty, McKenzie, Martin, Netterfield, Cockayne & Dwarte, 1988). BN can have either the zinc-blende (diamond) structure or a graphite-like structure (Wyckoff, 1963), but it is clear from the presence of the two features referred to above that, of the two possibilities, the specimen has the graphite-based structure. High-resolution imaging confirms this.

A second example is a specimen of a-C, prepared by condensing carbon plasma from a vacuum arc on a graphite cathode (McKenzie, Martin, White, Liu, Sainty, Cockayne & Dwarte, 1988). The $G(r)$ is shown in Fig. 5(*e*), and clearly shows that the material has the diamond structure. On the other hand, annealed a-C:H (McKenzie, Cockayne, Dwarte & Turner, 1988) shown in Fig. 5(*f*) shows the graphite structure.

5.4. *Bond distortion*

Fig. 6 shows the $G(r)$ obtained for a number of tetrahedrally bonded amorphous semiconductors (a-Ge, a-Ge:H, a-Si:H, a-C and a-SiC:H). These materials have remarkably similar $G(r)$ despite the differences in the chemical properties of the various atoms and the presence in some of hydrogen. Table 2 shows the measured widths, at half-height, for the first-nearest-neighbour peak in $G(r)$ for each material, together with the width measured for the first-nearest neighbour of Pt. With the possible exceptions of a-SiC, the widths are the same as for Pt, indicating that the bond-length distortion in these materials is small, since the natural width of the first peak in Pt is determined essentially by thermal vibrations alone.

The instrumental and thermal broadening may be deconvoluted from the second peak, so that the natural breadth of the second peak is revealed. The results are shown in Table 2. In these tetrahedrally bonded semiconductors, this second-nearest neighbour corresponds to the edge of a tetrahedron. Because of the above result for first-nearest neighbours, distortions in the length of second-nearest neighbours can be interpreted as arising from bond-angle distortion. The relative bond-angle distortion may be found by dividing the natural width of the second peak by the bond length in each case. The results are again shown in Table 2. It is seen that a-C

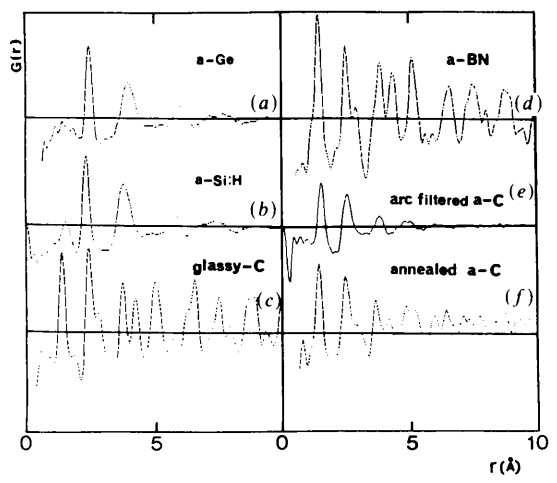

Fig. 5. $G(r)$ obtained for the materials shown.

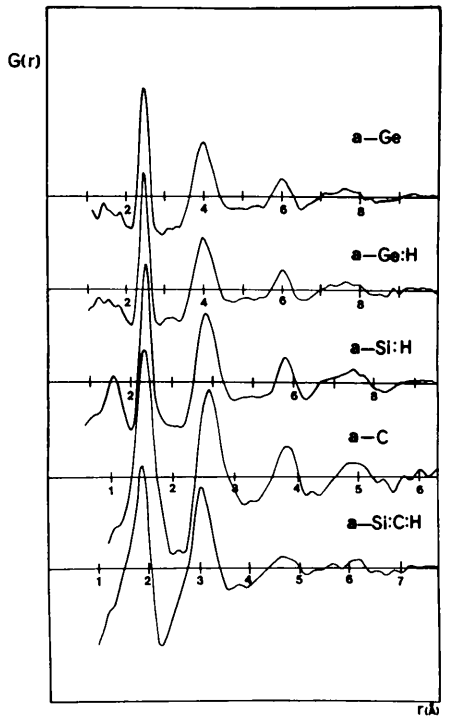

Fig. 6. $G(r)$ obtained for the materials shown, with r scaled in each case to bring the first-nearest neighbours into alignment.

has a smaller bond-angle distortion than the other materials. This result is understandable in view of the greater hardness of diamond, resulting from an increased stiffness of the tetrahedral bond angle. The bond-bending force constants for crystalline diamond, silicon and germanium are in the ratio 4·9:0·44:0·37 (Tomassini, Amore Bonapista, Lapiccirella, Lodge & Altmann, 1987), as determined by fitting lattice-dynamical results from neutron diffraction data.

The authors acknowledge financial support from the Australian Research Grants Committee without which development of the technique would not have been possible. The extensive assistance of D. Dwarte and Dr Z. Liu in developing and applying the techniques is acknowledged, and M. Lake is thanked for permission to refer to his work on Pt and alloys of Si and F. The specimen of glassy carbon was kindly supplied by Dr S. Prawer.

References

ANSTIS, G. R., LIU, Z. & LAKE, M. R. (1988). *Ultramicroscopy.* In the press.

BRIGHAM, E. O. (1974). *The Fast Fourier Transform.* Englewood Cliffs, New Jersey: Prentice Hall.

DOYLE, P. A. & TURNER, P. S. (1968). *Acta Cryst.* A**24**, 390-397.

EGERTON, R. F. (1986). *Electron Energy Loss Spectroscopy in the Electron Microscope.* New York: Plenum

GRACZYK, J. F. (1979). *Phys. Status Solidi. A*, **55**, 231-242.

GRACZYK, J. F. & MOSS, S. C. (1969). *Rev. Sci. Instrum.* **40**, 424-433.

GRIGOROVICI, R. (1973). In *Electronic and Structural Properties of Amorphous Semicondutors*, edited by P. G. LE COMBER & J. MORT, pp. 191-241. London: Academic Press.

GRIGSON, C. W. B. (1962). *J. Electron. Control*, **12**, 209-232.

JENKINS, G. M. & KAWAMURA, K. (1976). *Polymeric Carbons - Carbon Fibre, Glass and Char.* Cambridge Univ. Press.

KAPLOW, R., STRONG, S. L. & AVERBACH, B. L. (1965). *Phys. Rev.* **138**, A1336-A1345.

KEATING, D. T. (1963). *J. Appl. Phys.* **34**, 923-925.

KONNERT, J. H. & KARLE, J. (1973). *Acta Cryst.* A**29**, 702-710.

LAKE, M. R. (1988). PhD thesis. Univ. of Sydney, Australia.

MCKENZIE, D. R., COCKAYNE, D. J. H., DWARTE, D. M. & TURNER, P. S. (1988). *Philos. Mag. B.* Submitted.

MCKENZIE, D. R., MARTIN, P. J., WHITE, S. B., LIU, Z., SAINTY, W. G., COCKAYNE, D. J. H. & DWARTE, D. M. (1987). *Proc. E-MRS Meet.*, June 1987, pp. 203-206. Paris: Les Editions de Physique.

MOSS, S. C. & GRACZYK, J. F. (1969). *Phys. Rev. Lett.* **23**, 1167-1171.

REIMER, L. (1984). *Transmission Electron Microscopy.* Berlin: Springer.

SAINTY, W. G., MCKENZIE, D. R., MARTIN, P. J., NETTERFIELD, R. P., COCKAYNE, D. J. H. & DWARTE, D. M. (1988). *J. Appl. Phys.* In the press.

TOMASSINI, N., AMORE BONAPISTA, A., LAPICCIRELLA, A., LODGE, K. W. & ALTMANN, S. (1987). *J. Non-Cryst. Solids*, **93**, 241-256.

WARREN, B. E. (1969). *X-ray Diffraction.* Reading, MA: Addison-Wesley.

WYCKOFF, R. W. G. (1963). *Crystal Structures.* New York: Interscience.

Acta Cryst. (1988). A**44**, 878-884

Validity Domain of the Weak-Phase-Object Approximation for Electron Diffraction of Thin Protein Crystals

MING-HSIU HO* AND BING K. JAP

Division of Biology and Medicine, Lawrence Berkeley Laboratory, University of California, Berkeley, CA 94720, *USA*

AND ROBERT M. GLAESER†

Department of Biophysics and Medical Physics, and Division of Biology and Medicine, Lawrence Berkeley Laboratory, University of California, Berkeley, CA 94720, *USA*

(*Received* 30 *November* 1987; *accepted* 9 *March* 1988)

Abstract

The domain of validity of the weak-phase-object (WPO) approximation is evaluated for high-energy electrons (100 keV, 500 keV and 1 MeV) scattered by crystalline biological macromolecules. Cytochrome b_5 is used as an example in which calculated dynamical diffraction intensities are used to simulate observed diffraction intensities, which are then compared with intensities calculated by the weak-phase-object approximation. Three criteria of validity are used, namely the crystallographic residual (R value), the interpretability of difference Patterson maps, and the results of phasing by the heavy-atom isomorphous replacement method. The present calculations indicate that the error associated with the WPO approxi-

* Current address: Intermediate Voltage Electron Microscopy and Biomedical Image Analysis Resource, Department of Biology, University of Pennsylvania, Philadelphia, PA 19104, USA.

† To whom reprint requests should be addressed.

0108-7673/88/060878-07$03.00